Two-Step Spin Crossover in a Mononuclear Compound $[Fe(DPEA)(bim)](ClO_4)_2 \cdot 0.5\,H_2O$[DPEA = (2-Aminoethyl)-bis(2-pyridylmethyl)amine, bim = 2,2-Bisimidazole] − Crystal Structure, Magnetic Properties, Mössbauer Spectroscopy, and Photomagnetic Effects

Galina S. Matouzenko,*[a] Jean-François Létard,[b] Sylvain Lecocq,[c] Azzedine Bousseksou,[d] Laurence Capes,[b,e] Lionel Salmon,[d] Monique Perrin,[c] Olivier Kahn,[†][b] and André Collet[††][a]

Dedicated to the memory of André Collet and Olivier Kahn

Keywords: Iron / N ligands / Spin crossover / Mössbauer spectroscopy / Photomagnetism

The synthesis and characterization of the new spin crossover mononuclear complex $[Fe^{II}(DPEA)(bim)](ClO_4)_2 \cdot 0.5\,H_2O$, where DPEA = (2-aminoethyl)bis(2-pyridylmethyl)amine and bim = 2,2-bisimidazole, are reported. Variable-temperature magnetic susceptibility measurements (77–295 K) reveal the occurrence of a two-step spin transition. Two steps on the magnetic curve are separated by an inflection point at 200 K, corresponding to about 50% of the complexes that have undergone a thermal spin transition. The first step is centered at 171 K and the second one at 218 K. Mössbauer spectroscopy and X-ray analysis show that the profile of the magnetic curve is a consequence of the presence of two inequivalent iron(II) molecules in the crystal lattice. The crystal structure was resolved at 293 K (high-spin form) and at 123 K (low-spin form). Both spin-state isomers belong to the monoclinic space group $P2_1/c$ ($Z = 4$). The main differences between high-spin and low-spin isomers are found in the geometry of the $[FeN_6]$ core, the shorter Fe–N distances are seen at lower temperatures. Two inequivalent HS molecules at lattice sites **1** and **2** successively undergo a thermal spin transition. The analysis of the mean Fe–N distances for functionally different nitrogen donor atoms show that the two steps of the spin transition can be assigned to the inequivalent lattice sites. The gradual character of the spin transition at both lattice sites is accounted for in terms of intermolecular H-bonding via the perchlorate ions. At 10 K the light-induced excited spin state trapping (LIESST) effect is observed within the SQUID magnetometer cavity. Two critical temperatures T_c(LIESST) were recorded (36 K and 21 K) and are attributed to the lattice sites **1** and **2**.

Introduction

During the last few decades coordination chemistry has provided many examples of new iron(II) compounds exhibiting high-spin (HS, $^5T_2$) ↔ low-spin (LS, $^1A_1$) transitions, which have been extensively studied using various techniques.[1] The proximity of HS and LS electronic states in an isolated molecule, governed by the interplay between the electron-pairing energy and the ligand field, is a prerequisite for the occurrence of a spin transition. The change of the molecular equilibrium geometry accompanying a spin transition in the solid state occurs through intermolecular interactions, leading to more or less pronounced cooperative effects. Different intermolecular interactions such as H-bonding, π-stacking, van der Waals interactions can act as the communication link between neighboring molecules. Several theoretical models have been proposed to account for cooperativity in spin transition.[2]

The crystal structure plays an important role in the shaping of spin transition. Packing effects appear as a small perturbation on the interplay between the ligand field and the interelectronic interactions. Besides this they determine the propagation pattern of the cooperative interactions in the solid. The influence of packing effects on the spin-state of the complex is neither predictable, nor controllable and can

[†] Deceased on Dec. 7, 1999.
[††] Deceased on Oct. 26, 1999.
[a] Stéréochimie et Interactions Moléculaires (UMR CNRS and ENS-Lyon n° 5532), École Normale Supérieure de Lyon, 69364 Lyon Cedex 07, France
E-mail: Galina Matouzenko@ens-lyon.fr
[b] Laboratoire des Sciences Moléculaires, Institut de Chimie de la Matière Condensée de Bordeaux (UPR CNRS n° 9048), 33608 Pessac, France
[c] Laboratoire de Reconnaissance et Organisation Moléculaire (UMR 5078), Université Claude Bernard-Lyon 1, 69622 Villeurbanne Cedex, France
[d] Laboratoire de Chimie de Coordination (UPR CNRS n° 8241), 31077 Toulouse Cedex, France
[e] Motorola centre de recherche, Espace technologique Saint Aubin, 91193 Gif, France

  1434−1948/01/1111−2935 $ 17.50+.50/0

lead to different situations. One such situation involves the existence of several polymorphic modifications with differing magnetic behavior for a single compound.[3,4] Recently, we have isolated, under the same experimental conditions, three polymorphic modifications of the [Fe(DPPA)$(NCS)_2$] complex, where DPPA = (3-aminopropyl)bis(2-pyridylmethyl)amine.[4] A detailed study has revealed that one polymorph undergoes a gradual spin transition, the second remains high-spin at temperatures down to 4.5 K and the third exhibits a spin transition with hysteresis. Another situation arises when several crystallographically independent iron(II) sites co-exist in the same unit cell. The structural distinctions among iron(II) complexes can result in their different magnetic behavior. In the iron(II) complex $[Fe(mtz)_6](BF_4)_2$ (mtz = 1-methyl-1*H*-tetrazole), one site remains in the HS form until 4.2 K and the second undergoes a thermal spin transition.[5] Two lattice sites can be selectively converted into their spin isomers at low temperature by irradiating light at different frequencies. A similar feature was observed for $[Fe(etz)_6](BF_4)_2$ (etz = 1-ethyl-1*H*-tetrazole).[6] In the crystal of the iron(II) complex of C_3-cyclotriveratrylene ligand,[7] one site is occupied by LS species, whereas the other shows a temperature-independent mixture of HS and LS states. In the spin-equilibrium complex $[Fe(tren)](ClO_4)_2 \cdot {}^2/_3H_20$ [tren = tetrakis(2-pyridylmethyl)ethylendiamine)], one of two cation sites has a greater HS content, and both sites act quasi independently in the HS $\leftrightarrow$ LS conversion.[8] In the recently reported compound $[Fe(btr)_3](ClO_4)_2$ (btr = 4,4′-bis-1,2,4-triazole), the presence of two slightly different Fe^{II} sites generates the two-step spin transition with a plateau.[9] Another case of the two-step transition is represented by [Fe(5-NO_2-sal-N(1,4,7,10)] (the ligand results from the Schiff base condensation of 5-nitrosalicylaldehyde with tetraazadecane), in which two inequivalent lattice sites appear as a result of the structural phase transition on cooling.[10]

Here we report on the detailed characterization of a new spin transition complex $[Fe(DPEA)(bim)](ClO_4)_2 \cdot 0.5\ H_2O$, with DPEA = (2-aminoethyl)bis(2-pyridylmethyl)amine and bim = 2,2-bisimidazole (Scheme 1). The single-crystal X-ray structure at 293 K (HS form) and 123 K (LS form), magnetic susceptibility, Mössbauer spectra and photomagnetism of this complex are investigated. The presence of two inequivalent molecules in the crystal lattice both undergoing thermal spin conversion results in a two-step magnetic behavior. The LIESST (light-induced excited spin state trapping)[11] experiments reveal a partial conversion of the LS state into the HS state for both sites.

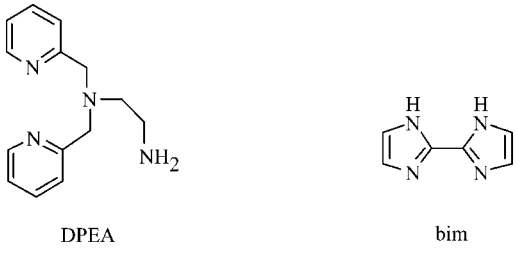

DPEA bim

Scheme 1. Representation of the DPEA and bim ligands

Results

Description of the Structure

The crystal structures of $[Fe(DPEA)(bim)](ClO_4)_2 \cdot 0.5\ H_2O$ in both HS and LS states were resolved by X-ray crystallography at 293 K and 123 K, respectively. The X-ray analysis did not reveal a change in the space group over the temperature range 123−293 K, and both spin-state forms belong to the monoclinic space group $P2_1/c$ (Z = 4). The unit cell contains two crystallographically independent iron(II) sites **1** and **2** (Figure 1), occurring in equal amounts in general positions. Selected bond lengths and angles are given in Table 1 and Table 2, respectively. The $[FeN_6]$ core is formed by two imino nitrogen atoms of 2,2-bisimidazole and by four nitrogen atoms of the tetradentate DPEA ligand. The latter is coordinated to the iron(II) atom via two pyridine nitrogen atoms in apical positions and by two aliphatic amino groups in adjacent positions. Thus, due to the meridionally arranged DPEA pyridine rings, both inequivalent iron(II) complexes represent the achiral *mer* isomer, as was also observed for $[Fe(DPEA)(NCS)_2]$.[12] Despite some

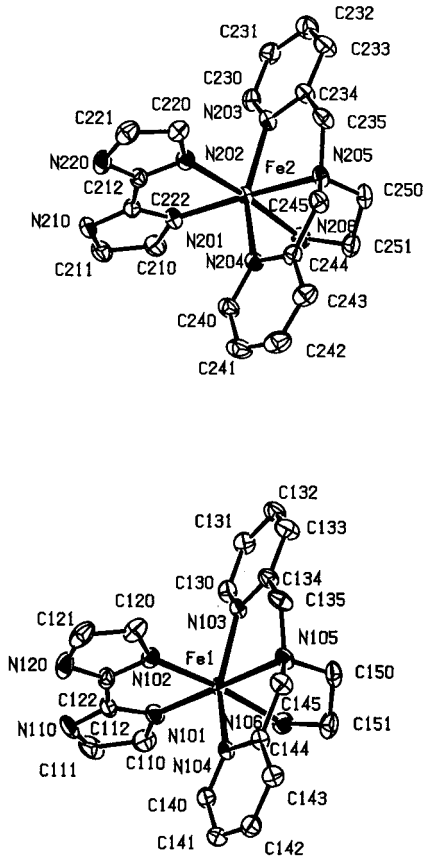

Figure 1. ORTEP view of the two inequivalent $[Fe(DPEA)(bim)](ClO_4)_2 \cdot 0.5\ H_2O$ molecules of the unit cell at 293 K (ellipsoids enclose 20% probability)

Table 1. Selected bond lengths [Å] for [Fe(DPEA)(bim)]-$(ClO_4)_2$·0.5 H_2O

	T = 293 K	T = 123 K
Fe(1)−N(101)	2.130(4)[a]	1.996(2)[a]
Fe(1)−N(102)	2.233(4)	2.040(3)
Fe(1)−N(103)	2.181(3)	1.979(2)
Fe(1)−N(104)	2.208(3)	1.989(3)
Fe(1)−N(105)	2.209(3)	1.991(2)
Fe(1)−N(106)	2.173(4)	2.012(3)
Fe(2)−N(201)	2.134(4)	1.993(2)
Fe(2)−N(202)	2.253(4)	2.060(3)
Fe(2)−N(203)	2.143(4)	1.964(2)
Fe(2)−N(204)	2.177(3)	1.977(2)
Fe(2)−N(205)	2.211(3)	1.994(2)
Fe(2)−N(206)	2.194(4)	2.021(3)

[a] Estimated standard deviations in the least significant digits are given in parentheses.

Table 2. Selected angles [deg] for [Fe(DPEA)(bim)]$(ClO_4)_2$·0.5 H_2O

	T = 293 K	T = 123 K
N(101)−Fe(1)−N(102)	77.5(2)[a]	80.7(1)[a]
N(101)−Fe(1)−N(103)	105.2(2)	98.1(1)
N(101)−Fe(1)−N(104)	101.7(2)	96.9(1)
N(101)−Fe(1)−N(105)	178.5(2)	179.6(1)
N(101)−Fe(1)−N(106)	99.2(2)	94.1(1)
N(102)−Fe(1)−N(103)	93.6(2)	92.9(1)
N(102)−Fe(1)−N(104)	87.6(2)	89.0(1)
N(102)−Fe(1)−N(105)	101.2(2)	99.3(1)
N(102)−Fe(1)−N(106)	174.0(2)	174.0(1)
N(103)−Fe(1)−N(104)	152.7(2)	165.0(1)
N(103)−Fe(1)−N(105)	75.6(2)	81.5(1)
N(103)−Fe(1)−N(106)	92.1(2)	90.8(1)
N(104)−Fe(1)−N(105)	77.4(2)	83.6(1)
N(104)−Fe(1)−N(106)	88.3(2)	88.7(1)
N(105)−Fe(1)−N(106)	82.1(2)	86.0(1)
N(201)−Fe(2)−N(202)	77.0(2)	80.5(1)
N(201)−Fe(2)−N(203)	107.9(2)	98.8(1)
N(201)−Fe(2)−N(204)	98.9(2)	95.6(1)
N(201)−Fe(2)−N(205)	176.1(2)	179.3(1)
N(201)−Fe(2)−N(206)	99.2(2)	93.8(1)
N(202)−Fe(2)−N(203)	92.6(2)	91.9(1)
N(202)−Fe(2)−N(204)	89.0(2)	90.2(1)
N(202)−Fe(2)−N(205)	101.8(2)	99.5(1)
N(202)−Fe(2)−N(206)	174.7(2)	174.0(1)
N(203)−Fe(2)−N(204)	152.8(2)	165.6(1)
N(203)−Fe(2)−N(205)	75.9(2)	81.9(1)
N(203)−Fe(2)−N(206)	92.1(2)	90.9(1)
N(204)−Fe(2)−N(205)	77.3(2)	83.7(1)
N(204)−Fe(2)−N(206)	88.0(2)	88.5(1)
N(205)−Fe(2)−N(206)	81.8(2)	86.2(1)

[a] Estimated standard deviations in the least significant digits are given in parentheses.

differences in the corresponding bond lengths and angles of the two inequivalent $[FeN_6]$ octahedrons, their configurations are the same at both temperatures.

(a) High-Spin Complex Structure (T = 293 K)

The similar $[FeN_6]$ octahedrons in the two inequivalent molecules are strongly distorted. The two Fe−N distances involving the 2,2-bisimidazole ligand are rather different [site **1**: Fe1−N101 = 2.130(4) Å, Fe1−N102 = 2.233(4) Å; site **2**: Fe2−N201 = 2.134(4) Å, Fe2−N202 = 2.253(4) Å]. The Fe−N(DPEA) bond lengths also differ considerably for the aromatic and aliphatic nitrogen donor atoms within each site and between both sites (see Table 1). The corresponding N−Fe−N angles at both lattice sites are rather similar (Table 2). They fall within 75.6(2)−107.9(2)° for adjacent nitrogen atoms and 152.8(2)−178.5(2)° for opposite nitrogen atoms, instead of 90 and 180° that would be observed in an ideal octahedron. The largest deviations from 90° are observed in the five-membered chelate rings (see Table 2). Evidently, this severe distortion of the $[FeN_6]$ core from O_h symmetry is due to the steric constraints caused by the coordination of the tetradentate and bidentate ligands.

The large values of the equivalent isotropic displacement parameter at room temperature reflect a disorder of the perchlorate anions and the solvent water molecules in the crystal. The disordered character of the packing of the ClO_4 groups is also displayed in the variation of the distances and angles. The Cl−O bond lengths in four ClO_4 groups arising from two sites are in the range 1.277(6)−1.420(5) Å. The angles Cl−O−Cl fall within the range 98.4(5)−120.6(6)°, instead of 109° for an ideal tetrahedron. It has not been possible to split the atom positions into several different orientations.

The crystal packing of [Fe(DPEA)(bim)]$(ClO_4)_2$·0.5 H_2O consists of alternate layers originating from the Fe1 and Fe2 molecule sets parallel to the *bc* plane. Figure 2 shows a projection of the structure along the *b* axis. Each layer can be considered as being formed by the columns of complex cations along the *b* direction. The columns of the complex cations at lattice sites **1** and **2** result from the symmetry operations ($-x$, $-{}^1/_2 + y$, ${}^1/_2 - z$) and ($1 - x$, $-{}^1/_2 + y$, ${}^1/_2 - z$), respectively. The nearest complexes in the columns are linked by π-stacking interactions resulting from a par-

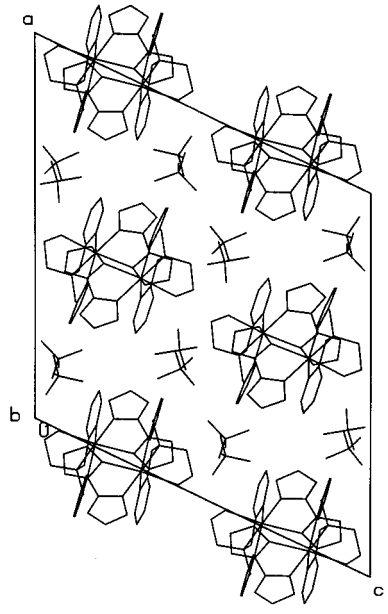

Figure 2. Projection of the molecular structure along the *b* axis at 293 K

Table 3. Intermolecular C···C contacts [Å] shorter than van der Waals distances (3.6 Å) and selected Fe−Fe distances for $[Fe(DPEA)(bim)](ClO_4)_2 \cdot 0.5\ H_2O$

	293 K	123 K
C(130)···C(143)[1] [a]	3.549(8)[b]	3.410(5)[b]
C(130)···C(144)[1]	3.597(8)	3.490(5)
C(131)···C(140)[1]	3.497(8)	3.563(5)
C(131)···C(141)[1]	3.544(9)	3.598(5)
C(132)···C(141)[1]	3.597(9)	3.461(5)
C(230)···C(243)[2]		3.471(5)
C(230)···C(244)[2]		3.519(5)
C(231)···C(240)[2]	3.417(8)	3.387(5)
C(231)···C(241)[2]	3.444(9)	3.455(5)
C(232)···C(241)[2]		3.447(5)
Fe(1)−Fe(1)[1]	7.455(1)	7.413(1)
Fe(1)−Fe(1)[3]	10.349(2)	10.232(2)
Fe(1)−Fe(1)[4]	11.258(2)	11.501(2)
Fe(1)[1]−Fe(1)[3]	14.093(3)	13.676(3)
Fe(2)−Fe(2)[5]	7.417(1)	7.394(1)
Fe(2)−Fe(2)[6]	10.208(2)	10.027(2)
Fe(2)−Fe(2)[7]	9.764(2)	9.460(2)
Fe(2)[5]−Fe(2)[6]	14.936(3)	14.863(3)

[a] Key: ([1]) $-x, -1/2 + y, 1/2 - z$; ([2]) $1 - x, -1/2 + y, 1/2 - z$; ([3]) $x, 3/2 - y, 1/2 + z$; ([4]) $-x, 1 - y, 1 - z$; ([5]) $1 - x, 1/2 + y, 1/2 - z$; ([6]) $x, 1/2 - y, 1/2 + z$; ([7]) $1 - x, 1 - y, 1 - z$. [b] Estimated standard deviations in the least significant digits are given in parentheses.

tial overlap of the pyridine rings of the DPEA ligand, which can be illustrated by the corresponding C···C intermolecular contacts (see Table 3). The dihedral angles between the stacked pyridine planes of the adjacent molecules are 9.6(4) and 20.2(4)° at lattice sites **1** and **2**, respectively. Each column is surrounded by perchlorate anions, yielding the electrically neutral layers of molecules. The solvent water molecules are inserted between the layers. The cohesion within a layer, as well as between neighboring layers is achieved by numerous H-bonds involving the oxygen atoms of the perchlorate ions. Moreover, these indirect H-bonds are realized either by means of the same oxygen atom of the perchlorate ion, or by the different ones. Detailed information on the hydrogen-bonding interactions is listed in Table 4.

(b) Low-Spin Complex Structure (T = 123 K)

The comparison of the HS and LS complex structures shows that the molecular configuration of the two forms essentially remains unchanged. The main difference between them involves the variation of the octahedral geometry of the $[FeN_6]$ core. The HS → LS transition is accompanied by the shortening of the Fe−N bond lengths, the degree of which is dependent on the chemical nature of the nitrogen atoms. In the LS complex two Fe−N(bim) distances are shorter by 0.134 Å (Fe1−N101) and 0.193 Å (Fe1−N102) at lattice site **1**, relative to 0.141 Å (Fe2−N201) and 0.193 Å (Fe2−N202) at lattice site **2**. The reduction of the Fe−N(DPEA) mean distances to the aromatic and aliphatic nitrogen atoms at both lattice sites are 0.211 Å (Fe1−N_{arom}) and 0.190 Å (Fe1−N_{aliph}), and 0.190 Å (Fe2−N_{arom}) and 0.195 Å (Fe2−N_{aliph}). The N−Fe−N angles, which are significantly distorted in the HS complex, are closer to 90° and 180° in the LS complex. The range of the N−Fe−N angles for both lattice sites in the LS $[FeN_6]$ core is 80.5(1)−99.5(1)° and 165.0(1)−179.6(1)°. Clearly, the HS → LS transition is followed by the rearrangement of the $[FeN_6]$ octahedron into a more regular geometry.

The perchlorate anion positions, which are disordered at high temperatures, are far less perturbed at low temperature. The Cl−O distances are in the range 1.372(4)−1.445(3) Å. The Cl−O−Cl angles range from 104.9(2) to 113.4(4)°, and approach the regular tetrahedron value. The disordered nature of the solvent water molecules, which is noted at room temperature, is also reduced at low temperatures.

The crystal packing in the LS complexes is similar to that in the HS state, but more compact. This is consistent with the decrease in the volume of the unit cell by 5.66% and the increase in the density from 1.600 to 1.696 g/cm^3 on lowering the temperature to 123 K. In the columns of the

Table 4. Interatomic distances [Å] and angles [deg] for the hydrogen-bonding interactions for $[Fe(DPEA)(bim)](ClO_4)_2 \cdot 0.5\ H_2O$

D−H···A[a]	D−H	H···A[b]	D···A[b]	D−H···A[b]
293 K				
N(106)−H(10A)···O(42)[1]	0.900	2.546(14)	3.277(13)	138.7(3)
N(106)−H(10B)···O(23)[2]	0.900	2.424(8)	3.197(8)	144.1(2)
N(110)−H(110)···O(13)[2]	0.860	2.512(10)	3.135(9)	130.0(2)
N(120)−H(120)···O(20)[3]	0.860	2.449(9)	3.044(8)	126.9(2)
N(120)−H(120)···O(22)[3]	0.860	2.401(11)	3.151(9)	144.8(3)
N(206)−H(20A)···O(33)[4]	0.900	2.360(10)	3.144(9)	145.6(3)
N(206)−H(20B)···O(10)[2]	0.900	2.288(10)	3.104(10)	150.6(5)
N(210)−H(210)···O(13)[5]	0.860	2.246(9)	3.056(9)	157.1(2)
N(220)−H(220)···O(13)[5]	0.860	2.289(9)	3.086(9)	154.3(2)
C(111)−H(111)···O(30)[6]	0.930	2.563(11)	3.430(11)	155.2(3)
C(150)−H(15B)···O(23)[1]	0.970	2.594(8)	3.426(8)	143.9(2)
C(211)−H(211)···O(40)[7]	0.930	2.565(12)	3.337(11)	140.7(3)
C(233)−H(233)···O(42)[8]	0.930	2.548(16)	3.465(16)	168.7(3)
C(245)−H(24A)···O(12)[4]	0.970	2.412(11)	3.348(10)	162.1(3)
C(250)−H(25B)···O(12)[4]	0.970	2.549(11)	3.474(10)	159.3(3)
O(600)−H(600)···O(43)[7]	1.081	2.36(4)	3.15(2)	129(4)
123 K				
N(106)−H(10A)···O(41)[1]	0.900	2.549(6)	3.375(7)	159.5(1)
N(106)−H(10B)···O(23)[2]	0.900	2.280(5)	3.094(5)	150.3(1)
N(110)−H(110)···O(13)[2]	0.860	2.599(6)	3.229(6)	131.1(1)
N(120)−H(120)···O(20)[3]	0.860	2.222(5)	2.877(5)	132.8(2)
N(120)−H(120)···O(22)[3]	0.860	2.502(6)	3.219(6)	141.4(1)
N(206)−H(20A)···O(33)[4]	0.900	2.441(4)	3.197(6)	141.8(1)
N(206)−H(20B)···O(10)[2]	0.900	2.262(4)	3.126(4)	160.7(1)
N(210)−H(210)···O(13)[5]	0.860	2.158(5)	2.950(5)	152.9(1)
N(220)−H(220)···O(10)[5]	0.860	2.558(5)	3.316(5)	148.5(1)
N(220)−H(220)···O(13)[5]	0.860	2.308(5)	3.075(5)	147.6(1)
C(111)−H(111)···O(30)[6]	0.930	2.508(5)	3.355(5)	151.5(2)
C(210)−H(21A)···O(31)[7]	0.930	2.523(5)	3.426(5)	163.6(1)
C(221)−H(221)···O(31)[9]	0.930	2.547(5)	3.278(5)	135.8(1)
C(232)−H(232)···O(21)[8]	0.930	2.547(5)	3.317(5)	140.5(1)
C(233)−H(233)···O(42)[8]	0.930	2.386(6)	3.262(6)	156.9(1)
C(245)−H(24A)···O(12)[4]	0.970	2.401(5)	3.299(5)	153.8(1)
C(250)−H(25B)···O(12)[4]	0.970	2.514(5)	3.413(5)	154.2(1)
O(600)−H(601)···O(43)[7]	1.080	2.50(2)	3.30(1)	130(2)

[a] Symmetry operations: ([1]) $x, 1.5 - y, 0.5 + z$; ([2]) $-x, 0.5 + y, 0.5 - z$; ([3]) $-x, 1 - y, -z$; ([4]) $1 - x, 1 - y, 1 - z$; ([5]) $x, 0.5 - y, -0.5 + z$; ([6]) $-x, -0.5 + y, 0.5 - z$; ([7]) $x, -1 + y, z$; ([8]) $1 - x, -0.5 + y, 0.5 - z$; ([9]) $x, 1.5 - y, -0.5 + z$. [b] Estimated standard deviations in the least significant digits are given in parentheses.

cation complexes, the interplanar distances between the overlapping pyridine rings of the DPEA ligand are slightly reduced relative to the HS structure, as can be seen from the C···C intermolecular distances (Table 3). The dihedral angles between the adjacent stacked pyridine rings in the LS structure are reduced to 5.7(4) and 15.3(4)° at lattice sites **1** and **2**, respectively. It appears that in the LS structure the overlap between pyridine rings is more effective. As in the case of the HS form, no direct intermolecular interactions between the complexes from the different columns have been detected. The cohesion between the columns of complexes within a layer, as well as between the columns from neighboring layers, is maintained by numerous H-bonds. Data on the hydrogen-bonding interactions are listed in Table 4.

Magnetic Susceptibility Data

Variable-temperature magnetic susceptibility data were collected in both cooling and warming modes in the temperature range 290−77 K and are presented as $\chi_M T$ versus T plots in Figure 3. This magnetic behavior indicates a gradual spin transition between high-spin ($S = 2$) and low-spin ($S = 0$) electronic states. At 290 K, the magnitude of $\chi_M T$ is 3.13 $cm^3 \cdot mol^{-1} \cdot K$ ($\mu_{eff} = 5.01\ \mu_B$) which corresponds to a quintet spin-state. This value continuously decreases on cooling to 77 K, to reach a value of 0.02 $cm^3 \cdot mol^{-1} \cdot K$ ($\mu_{eff} = 0.40\ \mu_B$), which is close to the expected temperature-independent paramagnetism value for singlet spin state iron(II) complexes. Furthermore, the absence of residual paramagnetism at low temperatures, as confirmed by Mössbauer spectroscopy (vide infra), suggests that the spin transition is practically complete. Examination of the shape of the magnetic curve reveals that the spin transition takes place in two steps, separated by an inflection point at about 200 K. Approximately 50% of the complexes undergo a thermal spin transition at this temperature. The high-temperature and low-temperature steps are centered at about 218 and 171 K, respectively.

Mössbauer Spectroscopy

The temperature-dependent ^{57}Fe Mössbauer spectra of [Fe(DPEA)(bim)]$(ClO_4)_2 \cdot 0.5\ H_2O$ were recorded between 80 and 295 K. Figure 4 shows six relevant spectra obtained in the cooling mode. Fitting parameters for all spectra are given in Table 5. The low- and high-temperature spectra are characteristic for the LS and HS states of iron(II). According to the X-ray study (vide supra), the crystal lattice of [Fe(DPEA)(bim)]$(ClO_4)_2 \cdot 0.5\ H_2O$ incorporates two inequivalent iron(II) molecules with slightly different $[FeN_6]$ core geometries. The Mössbauer spectra also clearly agree with the presence of two spin crossover sites in the system.

The thermal variations of the quadrupole splitting and the isomer shift of the HS and LS doublets are shown in Figure 5. The thermal variation of the isomer shift of the LS and HS1 doublets is linear and follows the classical 2nd order Doppler shift law. The isomer shift of the HS2 doublet remains approximately constant between 80 and 295 K. The range of values (2.00−1.81 $mm \cdot s^{-1}$ for the first site and 2.4−2.0 $mm \cdot s^{-1}$ for the second site) of the quadrupole splitting ΔE_Q(HS) between 170 and 295 K is indicative of a strong distortion from cubic symmetry. This is also seen from the X-ray data, and suggests that the orbital levels are not degenerate. The orbital energy splittings can be obtained through the analysis of the thermal variation of the quadrupole splitting.[13] The ratio of the average energy splittings between the fundamental and first excited orbital states for the two sites ($\Delta E1$ and $\Delta E2$) gives a rough estimate of the relative degree of their distortion and can be evaluated from both the Ingalls's model[13] and ref.[10] and ref.[14] The ratio $\Delta E2/\Delta E1 = 0.74$ is obtained {$\Delta E = 570$ and 420 cm^{-1} and $\Delta E_Q(0\ K) = 2.06$ and 2.59 mm/s for sites **1** and **2**, respectively} when the thermal variation of the quadrupole splitting is fitted to the Ingalls's model[13] {$\Delta E_Q(T) = \Delta E_Q(0\ K) \times \tanh[\Delta E/2K_BT]$}. The same value for the ratio $\Delta E2/\Delta E1 = p_1/p_2 = 0.7$ was obtained from the slopes ($p_1 = 2 \cdot 10^{-3}$ $mm \cdot s^{-1} \cdot K^{-1}$ and $p_2 = 1.36 \cdot 10^{-3}$ $mm \cdot s^{-1} \cdot K^{-1}$) of the thermal variation of ΔE_Q(HS).[10,14] In systems with two non-equivalent Fe^{II} sites, the Mössbauer spectra would be expected to reveal two clearly separated quadrupole doublets. However, because of the temperature variation of the quadrupole splitting[10,14] and the similar

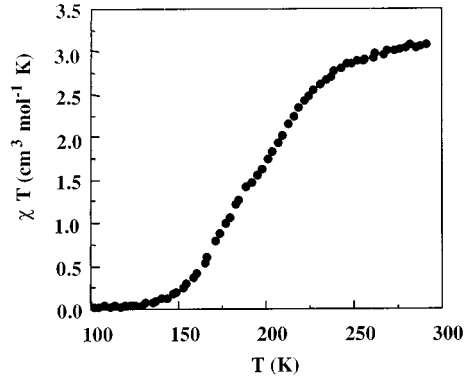

Figure 3. Thermal variation of $\chi_M T$ for [Fe(DPEA)(bim)]$(ClO_4)_2 \cdot 0.5\ H_2O$

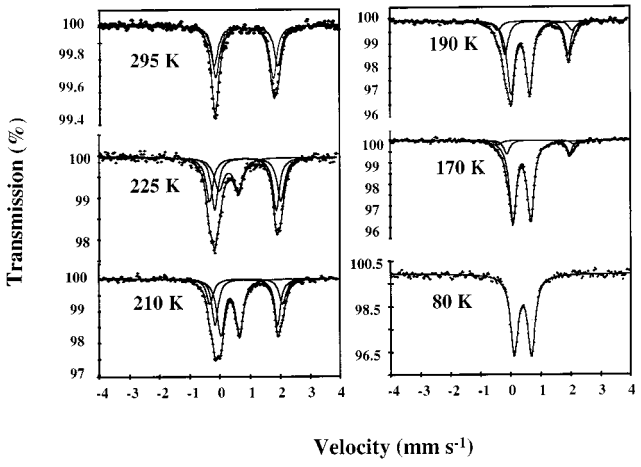

Figure 4. Selected Mössbauer spectra of [Fe(DPEA)(bim)]$(ClO_4)_2 \cdot 0.5\ H_2O$ recorded in the cooling mode. The solid lines represent fitted curves

Table 5. Least-squares-fitted Mössbauer data for $[Fe(DPEA)(bim)](ClO_4)_2 \cdot 0.5\ H_2O$

T	LS[a][b]			HS(1)			HS(2)			A_{HS1}/A_{tot}	A_{HS2}/A_{tot}	A_{LS}/A_{tot}
	δ	ΔE_Q^{LS}	$\Gamma/2$	δ	ΔE_Q^{HS}	$\Gamma/2$	δ	ΔE_Q^{HS}	$\Gamma/2$			
[K]	[mm·s^{-1}]	[mm·s^{-1}]	[mm·s^{-1}]	[mm·s^{-1}]	[mm·s^{-1}]	[mm·s^{-1}]	[mm·s^{-1}]	[mm·s^{-1}]	[mm·s^{-1}]	(%)	(%)	(%)
295	–	–	–	0.90(4)	1.81(8)	0.24(4)	0.96(4)	2.0(1)	0.28(4)	55(7)	45(7)	0
225	0.45(4)	0.61(4)	0.36(4)	0.99(1)	1.96(8)	0.24(4)	0.98(1)	2.2(1)	0.30(4)	41(7)	29(7)	30(1)
210	0.47(1)	0.60(1)	0.28(1)	1.00(1)	2.00(4)	0.24(2)	1.00(1)	2.3(1)	0.26(4)	33(3)	21(3)	46(1)
190	0.485(4)	0.59(3)	0.26(1)	1.01(1)	2.03(4)	0.25(2)	0.97(4)	2.4(2)	0.30(8)	28(2)	10(2)	62(1)
170	0.493(4)	0.57(1)	0.262(4)	1.02(3)	2.00(4)	0.22(4)	0.97(8)	2.4(2)	0.3(1)	12(2)	5(2)	83(1)
80	0.520(8)	0.55(1)	0.286(8)	–	–	–	–	–	–	0	0	100

[a] δ, isomer shift; ΔE_Q, quadrupole splitting; Γ half-height width of line; A/A_{tot}, area ratio. – [b] Error bars are given in parentheses; isomer shift values refer to metallic iron at 300 K.

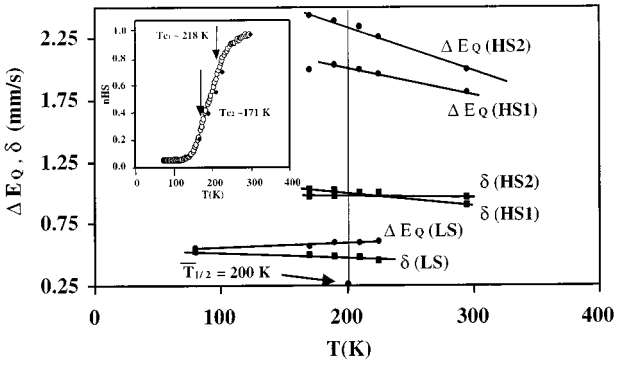

Figure 5. Thermal variation of the quadrupole splitting and the isomer shift of the HS and LS doublets obtained from the Mössbauer measurements of $[Fe(DPEA)(bim)](ClO_4)_2 \cdot 0.5\ H_2O$. In the inset: the thermal variation of the HS fraction (n_{HS}) obtained from magnetic susceptibility measurements (○) and the relative area of the HS component in the Mössbauer spectra (•)

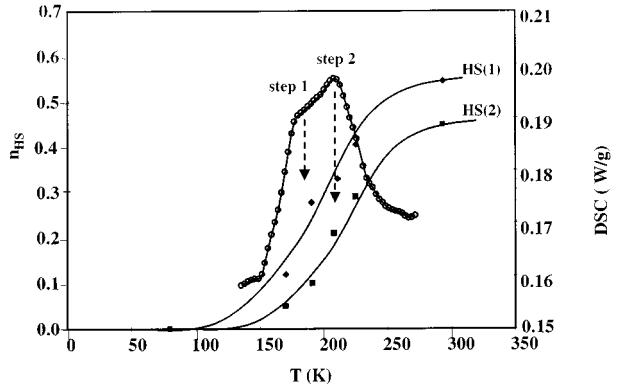

Figure 6. Thermal variation of the HS fractions for both lattice sites (◆ and ■) obtained by Mössbauer spectroscopy and the DSC curve (○) for $[Fe(DPEA)(bim)](ClO_4)_2 \cdot 0.5\ H_2O$

symmetries of the sites **1** and **2**, the two complexes cannot be easily separated. At high temperatures, the quadrupole splittings for the two sites with similar geometry almost merge, resulting in essentially one doublet.

On cooling, the $[Fe(DPEA)(bim)](ClO_4)_2 \cdot 0.5\ H_2O$ complex undergoes the HS → LS transition. On spin conversion the spectra show the co-existence of the HS and LS isomers, with strongly temperature-dependent relative intensities. At 80 K, the spectrum consists of one quadrupole doublet with typical parameters for the iron(II) LS state (Table 5), and the HS → LS transition at both **1** and **2** sites is complete, as seen by the absence of a residual HS fraction. The temperature at which 50% of the complexes undergo thermal spin transition is found to be close to 200 K. Curves showing the thermal variation of the total high-spin fraction n_{HS}, as determined from Mössbauer measurements and independently from magnetic susceptibility data, are in reasonable agreement as shown in the inset of Figure 5. In order to confirm the two-step character of the spin crossover, DSC measurements were carried out (Figure 6). Two peaks around 170 and 220 K are observed, which corresponds to the transition temperatures found from the thermal variation of the high-spin fraction for the two sites of the system obtained by Mössbauer spectroscopy (Figure 6). This confirms the two-step character of the spin transition in the present complex.

Photomagnetic Properties

The LIESST experiments were performed at 10 K on a very thin layer of powder sample. The weight was estimated by comparing the thermal spin crossover curve with the curve recorded with a heavier and accurately weighed sample. The sample was irradiated using different wavelengths accessible with the Laser-Diode (830±15 nm) and with the Kr^+ Laser; i.e. single-line 530.9 nm, multi-lines 647.1−676.4 nm and 752.3−799.3 nm.

At 10 K, the magnetic response of the sample without irradiation was diamagnetic (LS state). Irradiation with the wavelengths accessible with the Kr^+ Laser or the Laser-Diode resulted in a rapid increase of the magnetic response (Figure 7). This peculiar behavior may be assigned to a conversion into the HS state, according to the well-known LIESST effect.[11] It is worth noting that independent of the wavelengths used, the power applied and the irradiation time, the highest LS → HS conversion reached was about 40%. The optimal conversion was obtained with the multilines 647.1−676.4 nm at a power of 20 mW/cm^2 and after 2 hours of irradiation. In contrast, the irradiation of the compound at 830 nm induced only 5% of HS state, whereas tetrazole iron(II) derivatives exhibited a reverse-LIESST ef-

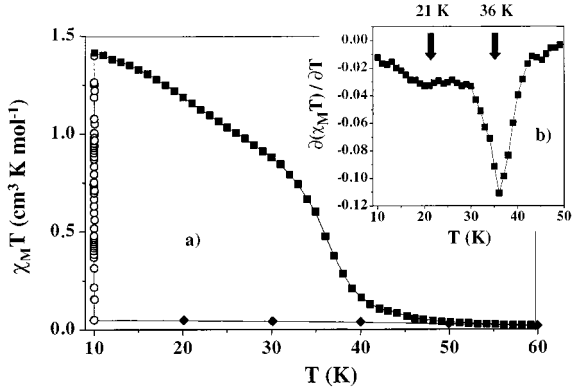

Figure 7. a) Temperature-dependence of $\chi_M T$ for [Fe(DPEA)(bim)]$(ClO_4)_2$·0.5 H_2O: (◆) data recorded in the cooling mode without irradiation; (○) data recorded with irradiation for 2 h at 10 K; (■) data recorded in the warming mode (0.3 K min^{-1}) after light irradiation was applied for two hours, then turned off. b) Derivative $\partial(\chi_M T)/\partial T$

fect instead.[15][11b] The most straightforward explanation for this difference is that the weak $^5T_2 \rightarrow {}^5E$ absorption band is totally overlapped by the intense ^{1}MLCT band involving the aromatic rings of the organic ligand.

We have recently proposed that the capacity of a compound to retain the light-induced HS information may be estimated through the determination of the T_c(LIESST) value.[16] By using the same procedure, we recorded the photomagnetic properties of [Fe(DPEA)(bim)]$(ClO_4)_2$·0.5 H_2O. After 2 hours of irradiation at 10 K, a photostationary limit was reached. The light was turned off and the temperature was slowly increased (0.3 K·min^{-1}). Figure 7 shows the temperature dependence of $\chi_M T$, which gradually decreases until 30 K and then rapidly drops to a value close to zero around 50 K. The $\partial(\chi_M T)/\partial T$ versus T plot reveals a clear minimum at a temperature of 36 K and also a second minimum is present around 21 K. This suggests that for both sites **1** and **2** the LS → HS conversion occurs under light-irradiation. The shape of the $\partial(\chi_M T)/\partial T$ vs. T plot nevertheless indicates a more effective LS → HS conversion for the site with the T_c(LIESST) at 36 K than for the site at 21 K.

Figure 8 shows the HS → LS relaxation curve recorded at 10 K. These data reveal a strong deviation from the single exponential law. The time-dependence of the high-spin fraction γ_{HS} is fast at first and then slows down. This behavior has been previously reported[17] and attributed to the local non-homogeneities of the iron(II) environment in the [FeN_6] core. Hauser et al.[17a] have proposed an analysis of the $\gamma_{HS}(t)$ curves based upon a distribution of relaxation rates $k_{HL}(T)$ and a corresponding repartition of the activation energy. In the [Fe(DPEA)(bim)]$(ClO_4)_2$·0.5 H_2O case, the situation is more complicated due to the population of sites **1** and **2**; i.e. each site may possess an exponential decay and hence the HS → LS relaxation curves may follow the bi-exponential law [Equation (1)].

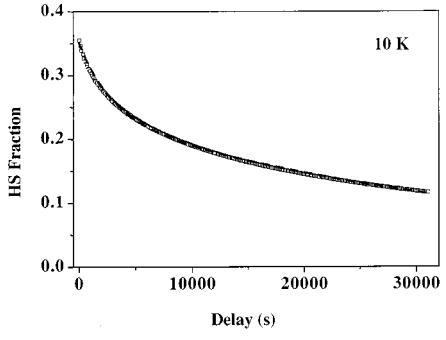

Figure 8. The HS → LS relaxation curve recorded at 10 K. The dashed line represents the fitted curve

$$\gamma_{HS} = A_1 \exp(-k_{HL}^1 t) + A_2 \exp(-k_{HL}^2 t) \quad (1)$$

The solid line shown in Figure 8 results from the least-squares fit of the relaxation data to Equation (1). It can be seen that a good fit of the data has been found with the biexponential law. The numerical fit results in values of $2.3 \cdot 10^{-5}$ s^{-1} and $3.4 \cdot 10^{-4}$ s^{-1} for k_{HL}, and of 0.24 and 0.11 for pre-exponential factors. Note that this relaxation curve can also be fitted by using a Gaussian distribution of activation energy centered at 50 cm^{-1} with a standard deviation of 12 cm^{-1} and a pre-exponential factor of $6.5 \cdot 10^{-2}$ s^{-1}. This gives a k_{HL} value of $5 \cdot 10^{-5}$ s^{-1}. However, the large standard deviation that arises in the latter case suggests that the bi-exponential analysis related to the two independent lattice sites is the more likely scenario.

Discussion

Relation Between the Structure and Spin Transition Properties

The synthesis and investigation of the title complex were undertaken with the aim of modifying the spin transition properties of the complex *mer*-[Fe(DPEA)$(NCS)_2$].[12] The latter manifests a sharp spin conversion close to the first-order transition. We expected that the replacement of two NCS groups by a bidentate ligand more predisposed to the intermolecular H-bonding, might enhance the cooperativity and eventually lead to a spin transition with hysteresis. The 2,2-bisimidazole molecule, containing two NH groups, was selected for this purpose. To the best of our knowledge, there are no data regarding iron(II) spin transition complexes with 2,2-bisimidazole in the literature. Contrary to expectation, the [Fe(DPEA)(bim)]$(ClO_4)_2$·0.5 H_2O complex exhibits a very gradual two-step spin transition which was revealed by the magnetic measurements, Mössbauer spectroscopy and differential scanning calorimetry. To date, there have been three reports in the literature describing the two-step behavior in spin crossover systems. The first one arises from the static density waves of HS complexes in the crystal lattice with a unique crystallographic Fe^{II} site.[18] The second one relates to binuclear complexes.[19] It is known that 2,2-bisimidazole can act not only as a bidentate chelating ligand but also as a bridging tetradentate one.[20] The third reason for the two-step behavior may be due to the presence of two inequivalent sites in the crystal lattice.

The X-ray analysis of [Fe(DPEA)(bim)]$(ClO_4)_2$·0.5 H_2O shows that the unit cell contains two inequivalent molecules with analogous configurations. The average Fe−N distances at both lattice sites **1** and **2** are almost identical and equal to 2.189 and 2.185 Å at 293 K, and 2.001 and 2.002 Å at 123 K, respectively. The closeness of the mean Fe−N distances in both inequivalent HS molecules does not allow the two steps of the spin transition, which arise on cooling, to be attributed to lattice sites **1** and **2**. In order to address this question we must analyze separately the bond lengths for three pairs of functionally distinct nitrogen atoms, which form the first coordination sphere of iron(II), namely, imidazolic imine, pyridinic imine and aliphatic amine types. In the HS state, the mean Fe−N(imidazole), Fe−N(pyridine), and Fe−N(amine) distances are 2.182, 2.195, and 2.191 Å, respectively at lattice site **1**, compared with 2.194, 2.160, and 2.203 Å, respectively at lattice site **2**. In other words, the mean Fe−N(pyridine) distance is shorter by 0.035 Å at site **2**, whereas the mean Fe−N(imidazole) and Fe−N(amine) distances at this same site are both longer by 0.012 Å. The occurrence of the spin transition depends on the magnitude of the ligand field strength, and the ligand field strength depends on the metal−ligand distance (as $\approx 1/r^5$) and on the nature of the donor atoms. Three functionally distinct types of nitrogen donor atoms contribute, in differing degrees, to the overall magnitude of the ligand field.[1d] The main contribution arises from the aromatic pyridine ligands, participating in both σ- and π-bonding interactions and favoring the LS state in iron(II) complexes. The contribution of the imine nitrogen atoms of 2,2-bisimidazole is much weaker due to the lack of aromaticity. Indeed, the $[Fe(bim)_3]SO_4$ complex is paramagnetic.[21] The ligand field produced by the aliphatic amine nitrogen atoms is still weaker and is entirely determined by σ interactions. It is clear that the spin transition sequence at lattice sites **1** and **2** is dependent on the difference in the Fe−N(pyridine) distances. The shorter mean Fe−N(pyridine) distance at lattice site **2** (by 0.035 Å) ensures a stronger overall ligand field and can be regarded as favoring the higher temperature spin conversion. However, it is unlikely that the inflection point near 200 K separates two successive and independent spin transitions. As it follows from the Mössbauer data, it results from the overlap of two gradual spin processes with close transition temperatures. Under such conditions the X-ray study near the inflection point, which proved to be useful in the case of the two sharp steps separated by a plateau,[9,10] cannot distinguish spin states at two lattice sites.

It could be noted that the order-disorder transition of both the solvent molecules and the perchlorate anions on cooling might also be a reason for the different change in spin state for the two sites. However, the intrinsic structural distinction of the two Fe^{II} sites found from the X-ray data, and resulting in the difference in the overall ligand field (also displayed by the two values of the crystal field distortion parameter) seems to be a more likely explanation for the two-step transition behavior.

The X-ray analysis confirms that our goal of generating a branched network of intermolecular links in the crystal lattice has been attained (Table 3 and Table 4). Nevertheless, the spin transition is rather gradual. Let us consider the structural features responsible for cooperative interactions in [Fe(DPEA)(bim)]$(ClO_4)_2$·0.5 H_2O. The layers of Fe1 and Fe2 molecules alternate parallel to the *bc* plane, forming two similar interpenetrating sublattices (Figure 2). The cooperativity within a sublattice is assured by two different types of intermolecular interactions. The pyridine rings of the DPEA ligand of neighboring complexes partially overlap resulting in the columns of π-stacked molecules extended along the *b* direction. The Fe−Fe distances in columns for two HS sublattices, 7.455(1) and 7.417(1) Å, are rather short in comparison with the values for several other spin-crossover systems.[22] At 123 K, the C···C intermolecular contacts become shorter and some new contacts appear (Table 3), probably due to a more parallel arrangement of the pyridine rings. The second type of intermolecular interactions is represented by hydrogen-bonds (Table 4), forming a branched network. The H-bonds propagate preferentially in the *a* and *c* directions where they link the complexes of neighboring columns from the same or from different sublattices. The H-bonds between the molecules within the columns are less numerous. All hydrogen-bonds between the complexes are indirect and pass through the oxygen atoms of the perchlorate anions. As a result, the corresponding Fe−Fe distances are rather long and vary in the range 9.764(2)−14.936(3) Å within the HS sublattices and 9.466(2)−20.234(5) Å between them. The majority of the H-bonds involve the atoms belonging to the second coordination sphere of the Fe^{II} ion. Only four of the sixteen hydrogen-bonds include the nitrogen atoms directly linked to Fe^{II} and can be represented schematically as N−H···O(ClO_4) or N−H···O(ClO_4)···H−C. At 123 K, several new H-bonds appear but the overall network essentially does not change relative to the HS state. The indirect character of the hydrogen-bonds and the non-branched one-dimensional system of the intermolecular π-stacking do not provide a good basis for a strong cooperativity resulting in a gradual spin transition in [Fe(DPEA)(bim)]$(ClO_4)_2$·0.5 H_2O. It can reasonably be concluded that the various ways referred to above of propagating intermolecular interactions are responsible for the anisotropy in the unit cell contraction (2.15, 0.03, and 1.94% for the *a*, *b*, and *c* axes, respectively) on cooling.

Two distinct iron(II) lattice sites are also manifested in the LIESST process. The HS conversion after light irradiation at 10 K results in the two minima in the $\partial(\chi_M T)/\partial T$ versus T plot (Figure 7). The corresponding T_c(LIESST) values are 21 K and 36 K, with a less pronounced minimum for the first temperature. This shows that the relaxation at one of the two lattice sites is faster than at the other. The lifetime of the HS species at 10 K was recorded over a 10-hour period. As has already been reported for other spin crossover compounds exhibiting a LIESST effect, the HS → LS relaxation curves deviate markedly from single exponential behavior. The numerical data can be fitted both by

using a Gaussian distribution of activation energy and with a biexponential decay that considers two independent lattice sites. In this latter case, the numerical analysis shows that one of the two lifetimes is very short. This may explain why the HS conversion does not exceed 40%. In fact, the photostationary point reached after irradiation is due to a critical balance between light population and HS → LS relaxation.

According to the theory of nonadiabatic multiphonon relaxation,[23] the characteristic features of the relaxation rate constant are a temperature-independent tunneling rate at low temperatures and a thermally activated process at elevated temperatures. At low temperatures, the lifetimes of the HS species depend on both the Huang−Rhys factor, S, which is a measure of the horizontal displacement of the potential wells of the HS and LS states, and the energy gap $\Delta E°_{HL}$ HL between the lowest vibronic levels of the HS and LS states. Hauser et al.[24] proposed that S does not vary to a large extent within the series of $[FeN_6]$ compounds, whereas the energy difference and thus the reduced energy gap $p = \Delta E°_{HL}/h\omega$ varies from $p < 1$ for samples with $T_{1/2}$ below 100 K to $p > 10$ for LS compounds. The thermal spin transitions in $[Fe(DPEA)(bim)](ClO_4)_2 \cdot 0.5\ H_2O$ located at 171 K for lattice site **1** and at 218 K for site **2** correspond to a higher $\Delta E°_{HL}$ HL (and thus p) value for site **2**. Note that the Δr_{HL} values recorded by X-ray diffraction are similar for the two lattice sites (0.188 and 0.183 Å), and hence S can be assumed to be quasi constant. According to the inverse energy-gap law reported for $[FeN_6]$ core compounds, the increase in the p factor between the two lattice sites enables the faster relaxation to be attributed to lattice site **2**. Consequently, T_c(LIESST) around 21 K corresponds to the relaxation of site **2**, and that at 36 K to site **1**. The relaxation rates estimated at 10 K with both the biexponential fit and the Gaussian distribution are in the range $10^{-4}-10^{-5}\ s^{-1}$. These values, as well as those observed recently for other $[FeN_6]$ compounds[17b] exceed the values predicted by the inverse energy-gap law[24] with $S \approx 50$. Generally, this discrepancy can be accounted for by large changes in the Fe−N bond lengths, which do not agree with the theoretical approximations. The Δr_{HL} change (≈ 0.19 Å) for $[Fe(DPEA)(bim)](ClO_4)_2 \cdot 0.5\ H_2O$ is in the same range as for other $[FeN_6]$ core compounds (0.16−0.21 Å). It is clear that the LIESST effect is controlled by many parameters, which are not all identified yet. More extensive studies should be carried out.

Experimental Section

Materials: All reagents and solvents used in this study are commercially available and were used without further purification. All syntheses involving Fe^{II} species were carried out in deoxygenated solvents under an inert atmosphere of N_2 using glovebox techniques. (2-Aminoethyl)bis(2-pyridylmethyl)amine (DPEA) was obtained according to the procedure we have recently reported.[12] 2,2-Bisimidazole (bim) was prepared as described previously.[25] ^1H NMR spectra were recorded in $CDCl_3$ on a Bruker AC200 spectrometer operating at 200 MHz. Elemental analyses (C, H N, Cl, and Fe determination) were performed at the Service Central de Microanalyse du CNRS in Vernaison.

Caution: The perchlorate salts of metal complexes with organic ligands are potentially explosive. Only small quantities of the compound should be prepared and handled with much care!

Synthesis of the Iron(II) Complex: $Fe(ClO_4)_2 \cdot 6\ H_2O$ (72.6 mg, 0.2 mmol) was dissolved in 8 mL of ethanol/methanol (5:1 mixture) and 2,2-bisimidazole (26.8 mg, 0.2 mmol) was added to it. A yellow solution was formed. After the addition of (2-aminoethyl)bis(2-pyridylmethyl)amine (48.4 mg, 0.2 mmol) in 2 mL of the same mixture of alcohols, the solution turned red-brown. The solution was filtered and allowed to stand overnight at room temperature, affording yellow-brown crystals of $[Fe(DPEA)(bim)](ClO_4)_2 \cdot 0.5\ H_2O$ which were collected by filtration, washed with ethanol, and dried in vacuum. The crystal used in the X-ray structure determination was selected from this sample. Yield: 56%. − $C_{20}H_{25}Cl_2FeN_8O_{8.5}$ (640.2): calcd. C 37.52, H 3.94, N 17.50, Cl 11.08, Fe 8.72; found C 37.68, H 3.98, N 17.74, Cl 11.22, Fe 8.77.

Magnetic Properties: Magnetic susceptibility measurements were carried out using two instruments: (i) A Manics DSM-8 fully automated Faraday-type magnetometer equipped with an DN-170 Oxford Instruments continuous-flow cryostat and a BE 15f Bruker electromagnet operating at ca. 0.8 Tesla and in the 80−300 K temperature range; (ii) a MPMS-55 QuantumDesign SQUID magnetometer operating at ca. 2 Tesla in the 2−300 K temperature range. Data were corrected for the magnetization of the sample holder and for diamagnetic contributions.

LIESST experiments were realized using a Spectra-Physics series 2025 Ker^+ laser system coupled through an optical fiber to the cavity of a MPMS-55 Quantum Design SQUID magnetometer. The wavelengths at 830±15 nm were generated using a Laser Diode SDS-2360-L2. The measurements were performed on a very thin layer of powder sample. The weight was estimated by comparing the thermal spin crossover curve with that for a heavier and accurately weighed sample.

Mössbauer Spectra: The variable-temperature Mössbauer measurements were obtained on a constant-acceleration spectrometer with a 50 mCi source of ^{57}Co (Rh matrix). The isomer shift values (δ) are given with respect to metallic iron at room temperature. The absorber was a sample of microcrystalline powder enclosed in a 2 cm diameter cylindrical plastic sample holder, the size of which had been determined to optimize the absorption. The variable-temperature spectra were obtained in the range 80−305 K, using a MD306 Oxford cryostat, the thermal scanning was monitored by an Oxford ITC4 servocontrol device (±0.1 K). Fitting parameters for all spectra (Table 5) were obtained by using a least-squares computer program.[26] The standard deviations of statistical origin are given in parentheses. As a Mössbauer fitting criteria, in order to get correct parameters of the Mössbauer spectra components for the present compound, it was important to find a good starting point for the fitting procedure. The spectrum at 210 K was selected for this goal, since it is the only case where two components of the HS state can be separated, even visually. Once this spectrum fits well, the starting points of the fitting procedure for other spectra were obtained smoothly and continuously varying the Mössbauer parameters.

Differential Scanning Calorimetry (DSC): Calorimetric measurements were obtained with a NETZSCH DSC-204 differential scanning calorimeter. The instrument was calibrated at solid cyclohexane transition and melting temperatures, and at the mercury melt-

ing temperature. 27 mg of the sample was used in an aluminium sample-holder. An identical aluminium holder was used as a reference. The scan rate of the measurements in the cooling and heating modes was 10 K·min^{-1}. The temperature values are measured with a ±0.4 K accuracy and the uncertainty on the enthalpy values is ±2%. All results were analyzed with an integrated PROTEUS Analysis computational program.

Solution and Refinement of the X-ray Structure: A Nonius Kappa CCD diffractometer was used for data collection. The selected crystal was mounted on a thin glass fiber. Two collections were made: one at the room temperature and the second at 123 K after a very slow decrease of the temperature with a cold nitrogen gas flow at a rate of 0.3 K·min^{-1}. From 10 frames with 1° steps, the initial set of cell parameters was obtained for each measurement. A total of 42881 reflections were collected at room temperature, of which 12124 unique reflections were used for the structure determination. The second collection at 123 K involved 45394 measured reflections of which 11793 unique reflections were used for the hypothesis and refinement. The structures were solved by direct method using the SHELXS-97 program.[27] The structures were then refined by the least-squares method using the SHELXL-97[28] with anisotropic temperature factors for all non-H atoms. The hydrogen atoms were introduced at calculated positions and refined riding on their carrier atoms. The final R factor [with $I > 2\sigma(I)$] has a value of 0.077 and 0.056 for both structures. Crystal data and refinement results are summarized in Table 6. The perspective view of the asymmetric unit containing two complex cations (Figure 1) has been calculated with PLATON.[29]

Crystallographic data for the structures reported in this paper have been deposited with the Cambridge Crystallographic Data Centre as supplementary publication no. CCDC- 162786 for structure at 293 K and CCDC-162787 for structure at 123 K. Copies of the data can be obtained free of charge on application to CCDC, 12 Union Road, Cambridge CB2 1EZ, UK [Fax: (internat.) + 44−1223/336-033; E-mail:deposit@ccdc.cam.ac.uk].

Acknowledgments

We deeply thank Professor J. J. McGarvey for his helpful suggestions to the present work. We are grateful for financial support from the European Commission for granting the TMR-Network "Thermal and Optical Switching of Spin States (TOSS)", Contract No. ERB-FMRX-CT98−0199. We thank J.-F. Meunier for technical assistance in the Mössbauer spectroscopy, magnetic and DSC measurements.

Table 6. Crystallographic Data for [Fe(DPEA)(bim)]-$(ClO_4)_2$·0.5 H_2O

	T = 293 K	T = 123 K
chem formula	$C_{40}H_{50}N_{16}Cl_4O_{17}Fe_2$	
fw	1280.46	
a, Å	21.146(4)	20.692(4)
b, Å	13.692(3)	13.688(3)
c, Å	20.398(4)	20.003(4)
β, deg	115.82(3)	117.72(3)
V, Å^3	5316(2)	5015(2)
Z	4	4
space group	$P2_1/c$	$P2_1/c$
λ, Å	0.71073	0.71073
ρ_{calc}, g·cm^{-3}	1.600	1.696
μ, cm^{-1}	8.31	8.81
R[a] $[I > 2\sigma(I)]$	0.077	0.056
wR_2[b] $[I > 2\sigma(I)]$	0.211	0.136

[a] $R = \Sigma(|F_o| - |F_c|)/\Sigma|F_o|$. − $wR = \{\Sigma[w(F_o^2 - F_c^2)^2]/\Sigma[w(F_o)^2]\}^{1/2}$.

[1] [1a] H. A. Goodwin, *Coord. Chem. Rev.* **1976**, *18*, 293−325. − [1b] P. Gütlich, *Struct. Bonding* **1981**, *44*, 83−164. − [1c] E. König, G. Ritter, S. K. Kulshreshtha, *Chem. Rev.* **1985**, *85*, 219−234. − [1d] H. Toftlund, *Coord. Chem. Rev.* **1989**, *94*, 67−108. − [1e] P. Gütlich, A. Hauser, *Coord. Chem. Rev.* **1990**, *97*, 1−22. − [1f] J. Zarembowitch, O. Kahn, *New J. Chem.* **1991**, *15*, 181−190. − [1g] E. König, *Struct. Bonding.* **1991**, *76*, 51−152. − [1h] P. Gütlich, A. Hauser, H. Spiering, *Angew. Chem. Ed. Engl.* **1994**, *33*, 2024−2053. − [1i]O. Kahn, *Molecular Magnetism*; VCH: New York **1993**. − [1j]O. Kahn, E. Codjovi, *Phil. Trans. R. Soc. Lond. A* **1996**, *354*, 359−379.

[2] [2a] C. P. Slichter, H. G. Drikamer, *J. Chem. Phys.* **1972**, *56*, 2142−2160. − [2b] R. Zimmermann, E. König, *J. Phys. Chem. Solids* **1977**, *38*, 779−788. − [2c] P. S. Rao, P. Ganguli, B. R. McGarvey, *Inorg. Chem.* **1981**, *20*, 3682−3688. − [2d] N. Sasaki, T. Kambara, *J. Chem. Phys.* **1981**, *74*, 3472−3481. − [2e] S. Ohnishi, S. Sugano, *J. Phys. C* **1981**, *14*, 39−47. − [2f] H. Spiering, E. Meissner, C. P. Köhler, E. F. Müller, P. Gutlich, *Chem. Phys.* **1982**, *68*, 65−71. − [2g] H. Spiering, N. Willenbacher, *J. Phys. Condens. Matter* **1989**, 10089−10105.

[3] [3a] E. König, K. Madeja, *Inorg. Chem.* **1967**, *6*, 48−55. − [3b] E. König, K. Madeja, K. J. Watson, *J. Am. Chem. Soc.* **1968**, *90*, 1146−1153. − [3c] A. Ozarowski, B. R. McGarvey, A. B. Sarkar, E. Drake, *Inorg. Chem.* **1988**, *27*, 627−635.

[4] G. S. Matouzenko, A. Bousseksou, S. Lecocq, P. J. van. Koningsbruggen, M. Perrin, O. Kahn, A. Collet, *Inorg. Chem.* **1997**, *36*, 5869−5879.

[5] [5a]P. Poganiuch, S. Decurtins, P. Gütlich, *J. Am. Chem. Soc.* **1990**, *112*, 3270−3278. − [5b] L. Wiehl, *Acta Crystallogr., Sect. B* **1993**, *49*, 289−303.

[6] R. Hinek, H. Spiering, D. Schollmeyer, P. Gûtlich, A. Hauser, *Chem. Eur. J.* **1996**, *2*, 1427−1434.

[7] G. Matouzenko, G. Vériot, J. P. Dutasta, A. Collet, J. Jordanov, F. Varret, M. Perrin, S. Lecocq, *New J. Chem.* **1995**, *19*, 881−885.

[8] H. R. Chang, J. K. McCusker, H. Toftlund, S. R. Wilson, A. X. Trautwein, H. Winkler, D. N. Hendrickson, *J. Am. Chem. Soc.* **1990**, *112*, 6814−6827.

[9] Y. Garcia, O. Kahn, L. Rabardel, B. Chansou, L. Salmon, J. P. Tuchagues, *Inorg. Chem.* **1999**, *38*, 4663−4670.

[10] D. Boinnard, A. Bousseksou, A. Dworkin, J. M. Savariault, F. Varret, J. P. Tuchagues, *Inorg. Chem.* **1994**, *33*, 271−281.

[11] [11a] S. Decurtins, P. Gütlich, C. P. Köhler, H. Spiering, A. Hauser, *Chem. Phys. Lett.* **1984**, *105*, 1−4. − [11b] S. Decurtins, P. Gütlich, K. M. Hasselbach, H. Spiering, A. Hauser, *Inorg. Chem.* **1985**, *24*, 2174−2178.

[12] G. S. Matouzenko, A. Bousseksou, S. Lecocq, P. J. van Koningsbruggen, M. Perrin, O. Kahn, A. Collet, *Inorg. Chem.* **1997**, *36*, 2975−2981.

[13] R. Ingalls, *Phys. Rev.* **1964**, *133A*, 787−795.

[14] A. Ducouret-Cérèse, F. Varret, *J. Phys. (Paris)* **1988**, *49*, 661−666.

[15] A. Hauser, *Chem. Phys. Lett.* **1986**, *124*, 543−548.

[16] J.-F. Létard, L. Capes, G. Chastanet, N. Moliner, S. Létard, J.-A. Real, O. Kahn, *Chem. Phys. Lett.* **1999**, *313*, 115−120.

[17] [17a] A. Hauser, J. Adler, P. Gütlich, *Chem. Phys. Lett.* **1988**, *152*, 468−472. − [17b] T. Buchen, P. Gütlich, *Chem. Phys. Lett.* **1994**, *220*, 262−266. − [17c] In LB film: J.-F. Létard, O. Nguyen, H. Soyer, C. Mingotaud, P. Delhaès, O. Kahn, *Inorg. Chem.* **1999**, *38*, 3020−3021. − [17d] A. Roubeau, J. G. Haasnoot, J. Linares, F. Varret, *Mol. Cryst. and Liq. Cryst.* **1999**, *335*, 541−550.

[18] [18a] H. Köppen, E. W. Müller, C. P. Köhler, H. Spiering, E. Meissner, P. Gütlich, *Chem. Phys. Lett.* **1982**, *91*, 348−352. − [18b] A. M. Greenaway, C. J. O'Connor, A. Schrock, E. Sinn,

Inorg. Chem. **1979**, *18*, 2692−2695. − [18c] M. Mikami, M. Konno, Y. Saito, *Chem. Phys. Lett.* **1979**, *63*, 566−569. − [18d] K. Kaji, M. Sorai, *Thermochim. Acta* **1985**, *88*, 185−190. − [18e] R. Jakobi, H. Spiering, P. Gütlich, *J. Phys. Chem. Solids* **1992**, *53*, 267−275. − [18f] C. P. Köhler, R. Jakobi, E. Meissner, L. Wiehl, H. Spiering, P. Gütlich, *J. Phys. Chem. Solids* **1990**, *51*, 239−247. − [18g] H. Spiering, T. Kohlhaas, H. Romstedt, A. Hauser, C. Bruns-Yilmaz, J. Kusz, P. Gütlich, *Coord. Chem. Rev.* **1999**, *190−192*, 629−647.

[19] [19a] J. A. Real, H. Bolvin, A. Bousseksou, A. Dworkin, O. Kahn, F. Varret, J. Zarembowitch, *J. Am. Chem. Soc.* **1992**, *114*, 4650−4658. − [19b] J. A. Real, I. Castro, A. Bousseksou, M. Verdaguer, R. Burriel, M. Castro, J. Linares, F. Varret, *Inorg. Chem.* **1997**, *36*, 455−464.

[20] [20a] S. W. Kaiser, R. B. Saillant, P. G. Rasmussen, *J. Am. Chem. Soc.* **1975**, *97*, 425−426. − [20b] S. W. Kaiser, R. B. Saillant, W. M. Butler, P. G Rasmussen, *Inorg. Chem.* **1976**, *15*, 2681−2694. − [20c] M. S. Haddad, D. H. Hendrickson, *Inorg. Chem.* **1978**, *17*, 2622−2625. − [20d] P. G. Rasmussen, O. H. Bailey, J. C. Bayon, *Inorg. Chem.* **1984**, *23*, 338−344.

[21] F. Holmes, K. M. Jones, E. G. Torrible, *J. Chem. Soc.* **1961**, 4790−4793.

[22] [22a] B. Gallois, J. A. Real, C. Hauw, J. Zarembowitch, *Inorg. Chem.* **1990**, *29*, 1152−1158. − [22b] J.-F. Létard, P. Guionneau, L. Rabardel, J. A. K. Howard, A. E. Goeta, D. Chasseau, O. Kahn, *Inorg. Chem.* **1998**, *37*, 4432−4441. − [22c] P. Guionneau, J.-F. Létard, D. S. Yufit, D. Chasseau, G. Bravic, A. E. Goeta, J. A. K. Howard, O. Kahn, *J. Mater. Chem.* **1999**, *9*, 985−994.

[23] E. Buhks, G. Navon, M. Bixon, J. Jortner, *J. Am. Chem. Soc.* **1980**, *102*, 2918−2923.

[24] [24a] A. Hauser, A. Vef, P. J. Adler, *Chem. Phys.* **1991**, *95*, 8710−8717. − [24b] A. Hauser, *Comment. Inorg. Chem.* **1995**, *17*, 17−39.

[25] H. Debus, *Annalen.* **1859**, *107*, 199−208.

[26] F. Varret, *Proceedings of the International Conference on Mössbauer Effect Applications.* Jaipar, India, **1981**; Indian National Science Academy: New Delhi, **1982**.

[27] G. M. Sheldrick, *SHELXS-97*, *Program for Crystal Structure Determination*; University of Göttingen: Germany, **1997**.

[28] G. M. Sheldrick, *SHELXL-97*, *Program for Crystal Structure Refinement*; University of Göttingen: Germany, **1997.**

[29] A. L. Spek, *PLATON, A Multipurpose Crystallographic Tool*; Utrecht University: Utrecht, The Netherlands, **1999**.

Received May 17, 2001
[I01178]